Large void size ~100 Mpc, peculiar velocities ~600 km s^{-1} ⇒ time for galaxy to cross void ~1600 Gyr >> age of universe ⇒ galaxies formed near present locations ⇒
Seeds of structure from early universe – see ch. 30.

Ch. 28 Active Galaxies

§28.1 Observations of Active Galaxies p. 1085

Seyfert galaxies (after Carl Seyfert, 1911-1960) are galaxies w/ very bright nuclei & emission lines.
Seyfert 1s have broad emission lines (Fig. 28.1), Seyfert 2s narrow (Fig. 28.2)
Mrk stands for galaxy catalog of E.B. Markarian (1913-1985).
Only a few × 0.1% of galaxies are Seyferts. They are usually spirals (Fig. 28.3)

p. 1087 The Spectra of Active Galactic Nuclei (AGN)

AGNs = Seyferts, radio galaxies, quasars, blazars, etc.
(Fig. 28.4) shows a typical spectral energy distribution (SED).

$$L_{\text{interval}} \propto \int_{\nu_1}^{\nu_2} F_\nu \, d\nu = \int_{\nu_1}^{\nu_2} \nu F_\nu \frac{d\nu}{\nu} = \int_{\nu_1}^{\nu_2} \nu F_\nu \, d\ln\nu = \ln 10 \int_{\nu_1}^{\nu_2} \nu F_\nu \, d\log_{10}\nu$$

$$(\ln\nu = \ln 10^{\log_{10}\nu} = \log_{10}\nu \ln 10)$$

So equal areas in SED plot of νF_ν vs $\log_{10}\nu$ ⇒ equal energies.
Most notable feature of AGN SEDs – it extends over ~10 orders of magnitude from $\nu = 10^{10}$ Hz (radio) to 10^{20} Hz (γ-ray).
It can often be decomposed into a thermal source (blackbody, low polarization) + nonthermal (power-law, some polarization).
(Fig. 28.5) shows how power-law produced by superposition of individual electrons spiraling around B-field lines emitting synchrotron radiation.

p. 1090 Radio Galaxies

Defined by extreme brightness at radio wavelengths.
(Fig. 28.6) Cygnus A at $d = 240$ Mpc (28.7) is optical HST image.
Ex 28.1.1 ⇒ $L_{\text{radio}} = 4.8 \times 10^{37}$ W ~ 3× $L_{\text{Milky Way}}$
They are divided into broad-line & narrow-line radio galaxies, BLRGs & NLRGs.

p. 1092 Radio Lobes & Jets

Cyg A (Fig 28.6) has radio lobes + jet connecting galaxy to one lobe.
(Fig. 28.8) shows lobes, strong jet, & weak counter-jet of NGC 6251.
(Fig. 28.9) shows windblown jets of NGC 1265 moving thru intracluster gas.
(Fig. 28.10) M87 & jets, showing evenly spaced knots emitting in radio, visible, & X-rays.
(Fig. 28.11) is Centaurus A, closest AGN at 4.7 h^{-1} Mpc

p. 1095 The Discovery of Quasars

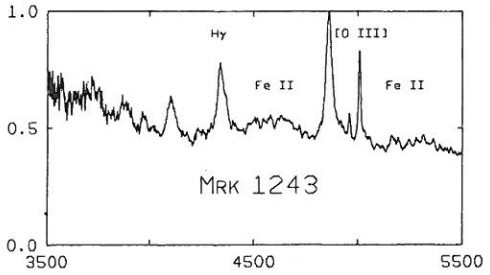

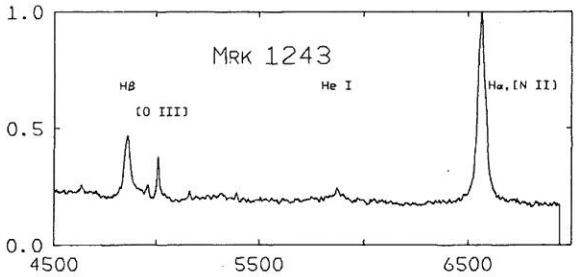

Fig. 28.1 Visible spectrum of Mrk 1243, a Seyfert 1 galaxy. Wavelengths in Angstroms.

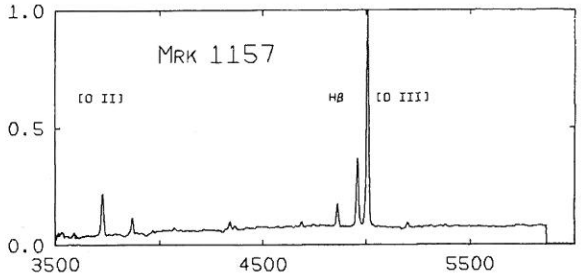

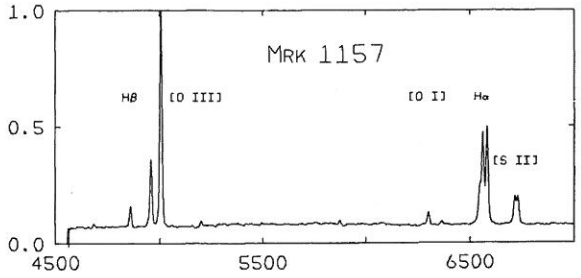

Fig. 28.2 Visible spectrum of Mrk 1157, a Seyfert 2 galaxy. Wavelengths in Angstroms.

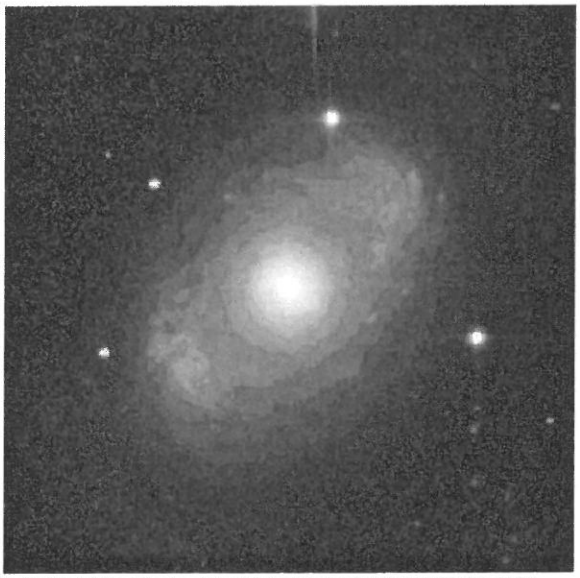

Fig. 28.3 Seyfert 1 (or 1.5) galaxy NGC 4151 showing galactic disk around bright nucleus.

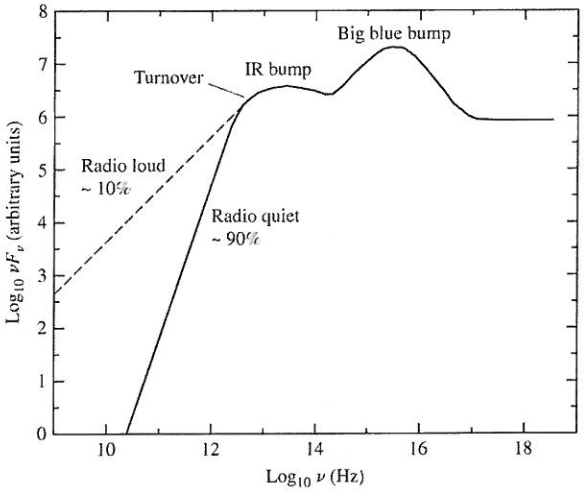

Fig. 28.4 A sketch of the continuum observed for many types of AGNs.

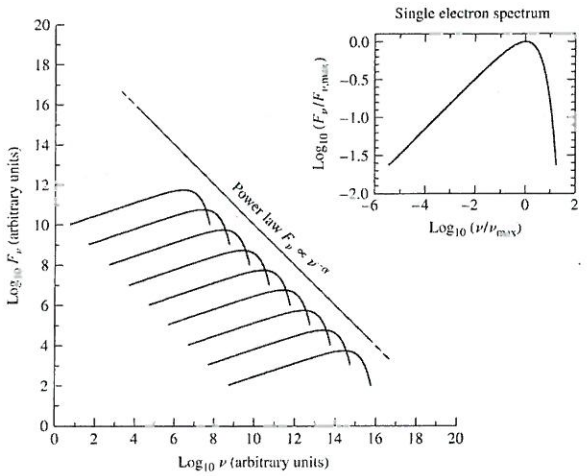

Fig. 28.5 The power-law spectrum of synchrotron radiation, shown as the sum of the radiation produced by individual electrons as they spiral around magnetic field lines. The spectrum of a single electron is in the upper right.

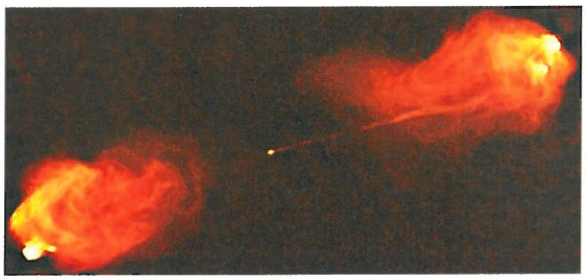

Fig. 28.6 A VLA image of Cygnus A, showing the two radio lobes separated by about $100h^{-1}$ kpc & the jet extending from the galaxy to the right-hand lobe. Cyg A is a narrow-line radio galaxy. The central cD galaxy does not show up on this radio picture.

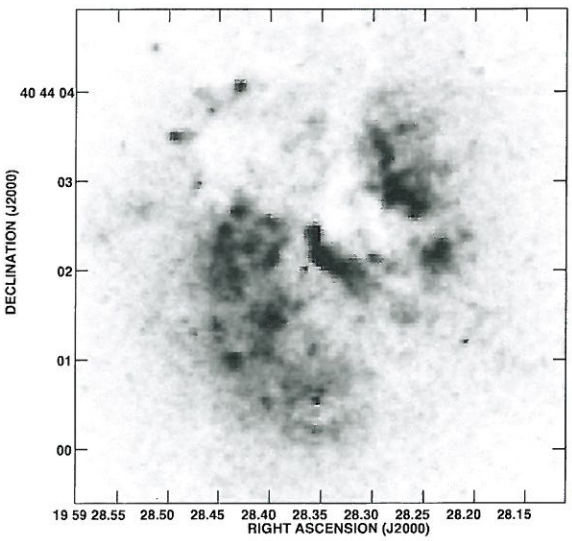

Fig. 28.7 A continuum image of Cyg A (3C 405) at $\lambda = 622$ nm.

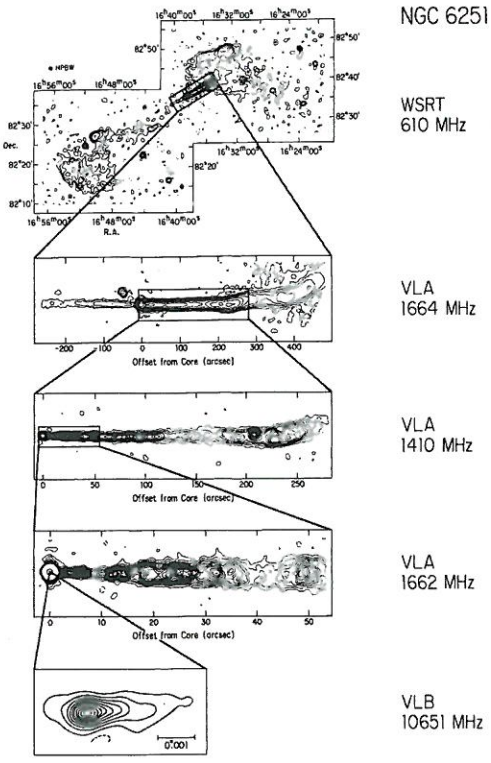

Fig. 28.8 The jet & counterjet (2nd panel) of radio galaxy NGC 6251.

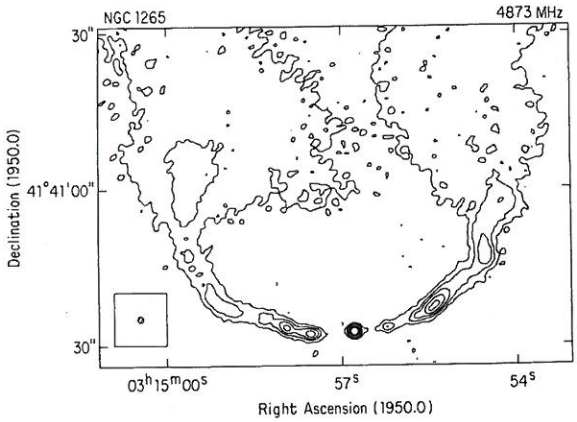

Fig. 28.9 Radio appearance of NGC 1265, with its jets swept back by that galaxy's motion through the surrounding intracluster gas.

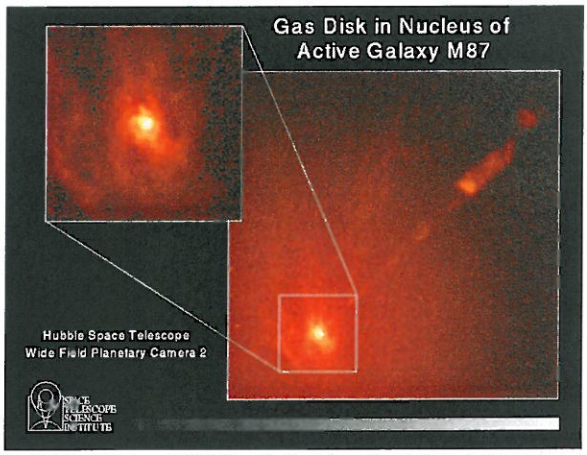

Fig. 28.10 Two HST views of M87 & its jet. The insert shows the spiral-shaped disk of hot gas at the center of M87.

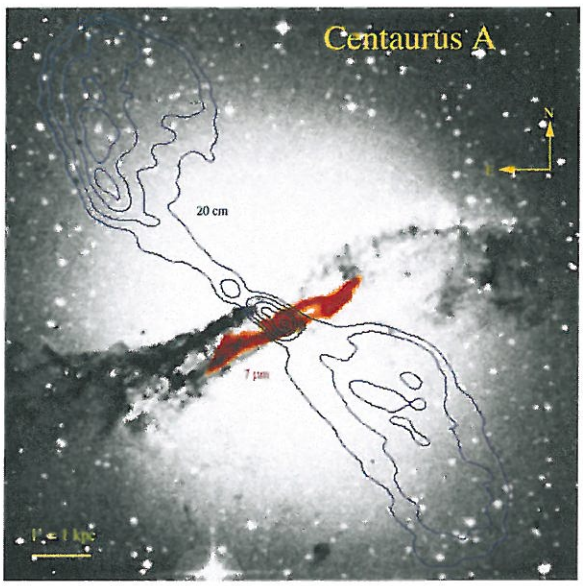

Fig. 28.11 The visual & radio appearance (superimposed contour lines) of radio galaxy Centaurus A.

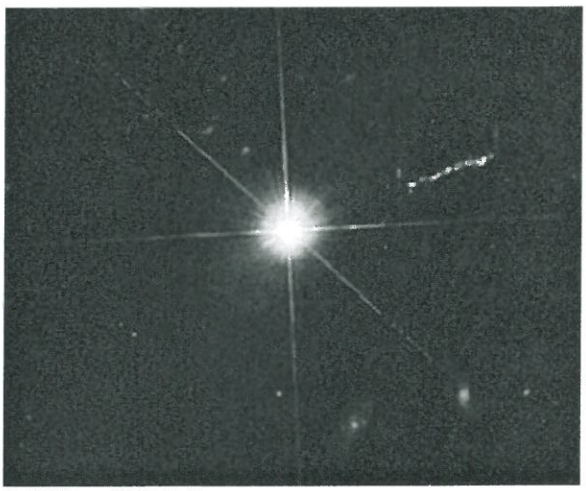

Fig. 28.12 Quasar 3C 273 & its jet

Astronomers looked for optical counterparts to strong radio sources, found starlike objects w/ unique spectra, named them quasi-stellar radio sources - quasars.

→ (Fig. 28.12) Quasar 3C 273 & its jet.

Soon Dutch astronomer Maarten Schmidt recognized that the lines H, but severely redshifted, $z = 0.158$, & soon 3C 48 was found to have $z = 0.367 \Rightarrow v = 0.303c$, $d = 900 h^{-1}$ Mpc - one of the most distant objects. (Fig. 28.13)

p. 1097 Quasar Luminosities

Ex. 28.1.2 3C 273 has $V = 12.8$, $d = 620$ Mpc $\Rightarrow$

(Eq. 3.6) $M_V = V - 5 \log_{10}\left(\frac{d}{10\text{ pc}}\right) = -26.2$

(Eq. 3.7) $L_V = 100^{(M_{sun} - M_V)/5} L_\odot = 2.6 \times 10^{12} L_\odot = 1 \times 10^{39}$ W

Typical $L_{bol} = 10^{38-41}$ W ~ $10^5 \times$ Milky Way.

Quasar Spectra

(Fig. 28.14) Large amounts of energy emitted over 5 orders of magnitude in V.

p. 1099 Quasi-Stellar Objects

Looking at all objects with excess UV luminosity $\Rightarrow$ 90% are relatively radio-quiet $\Rightarrow$ refer to them as quasi-stellar objects (QSOs) rather than quasars (QSRs).

Quasar Terminology

Commonly use quasar to refer to both radio-loud & radio-quiet.

Ultraluminous Infrared Galaxies - skip

The High Cosmological Redshifts of Quasars

The Sloan Digital Sky Survey (SDSS) has cataloged 46,420 quasars. Most distant has $z = 5.4135$. 520 have $z > 4$.

$\Rightarrow$ shouldn't interpret them as Doppler.

Wavelengths have lengthened by same ratio as universe $\Rightarrow$

$$z = \frac{\lambda_{obs} - \lambda_{emitted}}{\lambda_{emitted}} = \frac{R_{obs} - R_{emitted}}{R_{emitted}} \Rightarrow \frac{R_{obs}}{R_{emitted}} = 1 + z$$

$z = 3 \Rightarrow$ universe is 4x larger than when light emitted.

p. 1100 Evidence for Quasar Evolution

Number & brightness of quasars may change w/ time & this is complicated by fact that volume of space expands as $(1+z)^3 \Rightarrow$ define comoving space density which is density $/(1+z)^3$.

Statistical studies $\Rightarrow$ there are 1000x as many quasars/Mpc^3 (comoving) w/ $M_B < -25.9$ at $z = 2$ than now.

But total # of quasars has not changed since $z = 2$. (Fig. 28.15) Fig. 28.16 ↑

All curves same if shifted horizontally $\Rightarrow$ individual quasars dim w/ time after $z = 2$.

Comoving density peaks at $z \sim 2.5$ & drops off for $z > 3$. (Fig. 28.17)

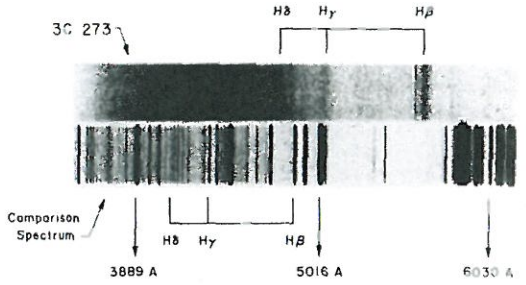

Fig. 28.13 The z=0.158 redshift of quasar 3C 273

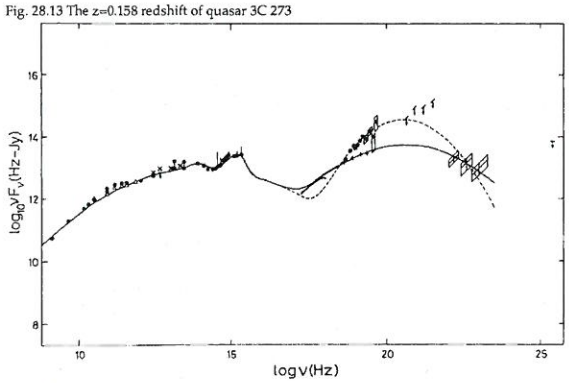

Fig. 28.14 The spectrum of 3C 273 after Doppler shift due to Hubble flow has been removed. A horizontal line would correspond to spectral index $\alpha = 1$; for reference, the diagonal dashed line shows the slope for F_ν = constant. The 2 lines on right correspond to 3C 273 during quiescence & during an outburst.

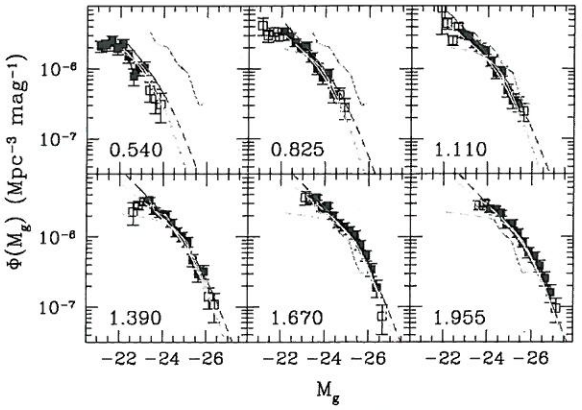

Fig. 28.15 Luminosity functions for quasars with different redshifts. Redshifts are indicated in each frame. The jagged line that is present in every frame represents the data for z = 1.390. Notice that the population is brighter at greater redshifts.

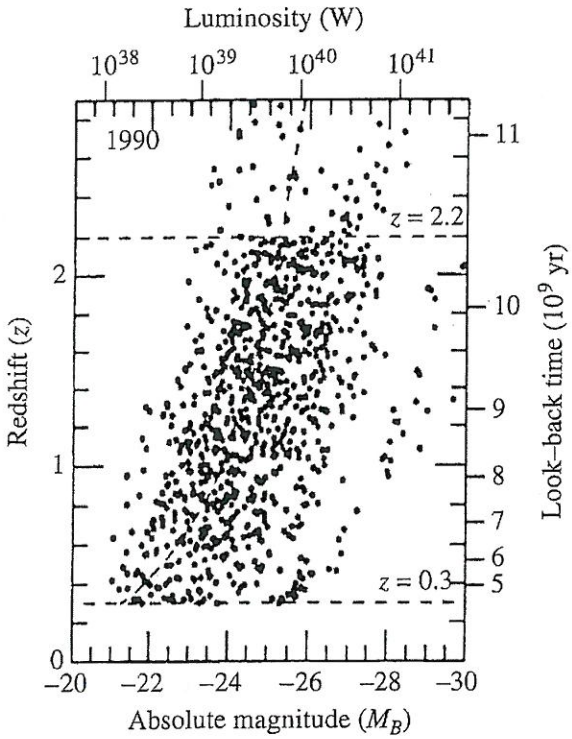

Fig. 28.16 The dimming of quasars with time.

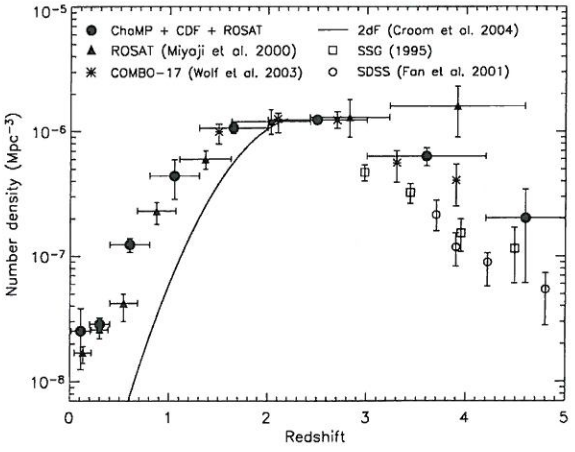

Fig. 28.17 The comoving space density of active galactic nuclei as a function of redshift.

this may indicate the growth phase of the SMBHs that power AGNs. There is evidence that a quasar "event" lasts only ~1 dynamical timescale ~ free-fall or orbital time.

(Fig. 28.18) Quasar in gravitational interaction w/ companion galaxy (visible as bright spot in book but not in image file) – curved wisps probably tidal interaction. Radio-loud quasars contain SMBHs w/ $M > 10^9 M_\odot$, radio-quiet $M > 5\times10^8 M_\odot$. ⇒ loud less abundant than quiet because loud requires higher M_{BH}.

Also find that $L \sim 0.15 - 0.5\, L_{Ed}$ ⇒ accretion power

p. 1104 Timescales of AGN Variability

L fluctuates by ×2 in months, weeks, or even days

Fig. 28.19 3C 279 brightened by ×250 ~1937.

Polarization of the Emission

(Fig. 28.20) B-field in lobes of 3C 47 as inferred from polarization.

p. 1105 Fanaroff–Riley Luminosity Classes – Skip

Blazars

Defined as AGNs w/ rapid variability (doubling in days or weeks) + high linear polarization, BL Lac objects named after BL Lacerta (lizard) – rapid variability – up to 30% in 24 hrs + ×100 over longer time period.

p. 1106 LINERS – Skip.

p. 1107 A Summary of AGN Classifications

(Table 28.1)

§28.2 A Unified Model of Active Galactic Nuclei

It now seems that all AGN powered by accretion onto SMBH, + differences are due to differences in viewing direction, $\dot{M}$, + M_{BH}.

Toward a Unified Model of AGNs

(Fig. 28.21) Hα emission lines presumably formed by photoionization of H by continuum, then recombination → $L_{H\alpha} \propto L_{FC}$ ⇒ straight line.

So all these different types of AGN are similar.

p. 1109 The Nature of the Central Engine

(Fig. 28.22) Optically thick sphere of radius R suddenly brightens.

Observed brightening occurs over $\Delta t = \frac{l_2 - l_1}{c}$ by light-travel time.

$l_2 = \frac{l_1 + R}{\cos\theta} \simeq l_1 + R \Rightarrow \Delta t = \frac{R}{c} \rightarrow R = c\Delta t$

If sphere moving away from us at v, calculated R becomes $R = c\Delta t\sqrt{1 - v^2/c^2} = \frac{c\Delta t}{\gamma}$

$\Delta t = 1$ day, $\gamma = 1 \rightarrow R = 1.1\times10^{12}$ m $= 7.2$ AU

$L < L_{Ed} \simeq 1.5\times10^{31} w\,(M/M_\odot)$

Typical $L = 5\times10^{39} w \Rightarrow M > 3.3\times10^8 M_\odot$

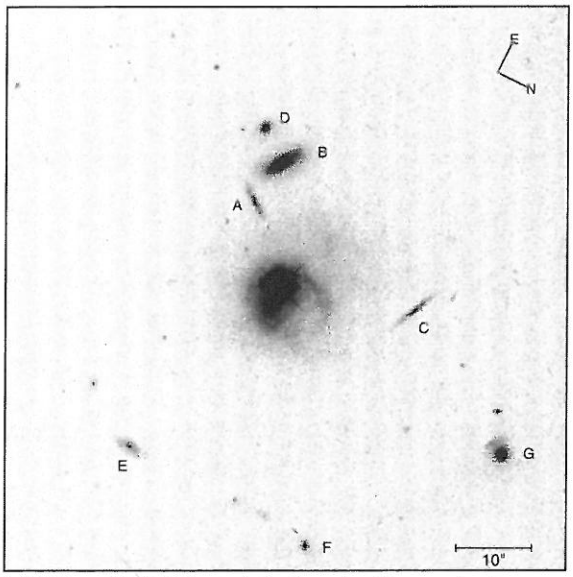

Fig. 28.18 Quasar PKS 2349–014 in a gravitational interaction with a companion galaxy.

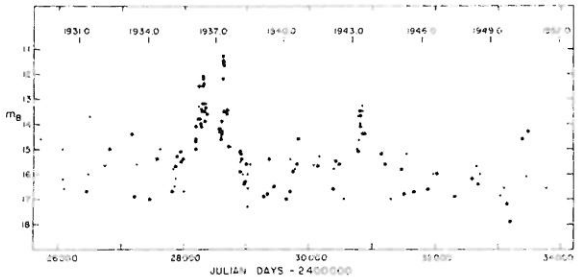

Fig. 28.19 Variation in apparent magnitude of quasar 3C 279, based on archival astronomical photographs

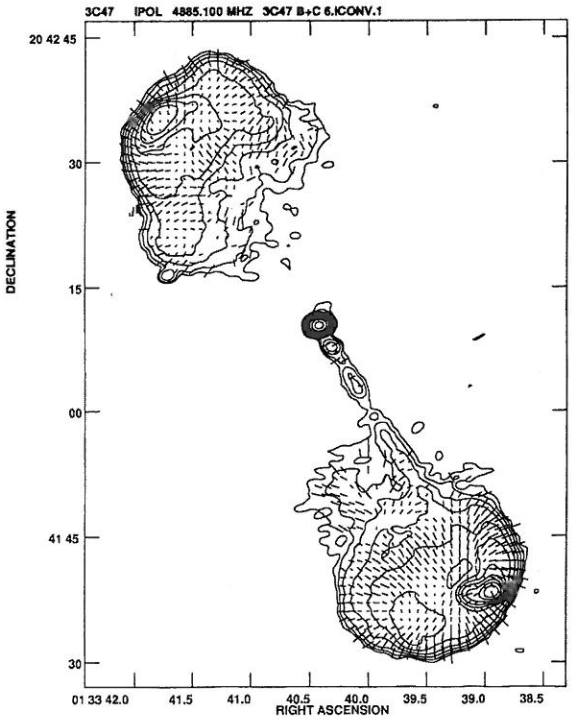

Fig. 28.20 Polarization mapping of the magnetic field of quasar 3C 47. Both lobes are highly polarized.

TABLE 28.1 A Summary of AGN Classes.

Class	Sub-class	Description
Seyferts	Type 1	broad and narrow emission lines, weak radio emission, X-ray emission, spiral galaxies, variable
	Type 2	narrow emission lines only, weak radio emission, weak X-ray emission, spiral galaxies, not variable
Quasars	Radio-loud (QSR)	broad and narrow emission lines, strong radio emission, some polarization, FR II, variable
	Radio-quiet (QSO)	broad and narrow emission lines, weak radio emission, weak polarization, variable
Radio Galaxies	BLRG	broad and narrow emission lines, strong radio emission, FR II, weak polarization, elliptical galaxies, variable
	NLRG	narrow emission lines only, strong radio emission, FR I and FR II, no polarization, elliptical galaxies, not variable
Blazars	BL Lacs	almost devoid of emission lines, strong radio emission, strong polarization, rapid variability, 90% in ellipticals
	OVV quasars	broad and narrow emission lines, strong radio emission, strong polarization, rapid variability, much more luminous than BL Lacs
ULIRGs		possibly dust-enshrouded quasars, alternatively may be starburst phenomena
LINERs		similar to low-luminosity Seyfert 2, low-ionization emission lines, in many (perhaps majority of) spiral galaxies, alternatively may be starburst phenomena or H II region emission

Table 28.1 A summary of AGN Classes

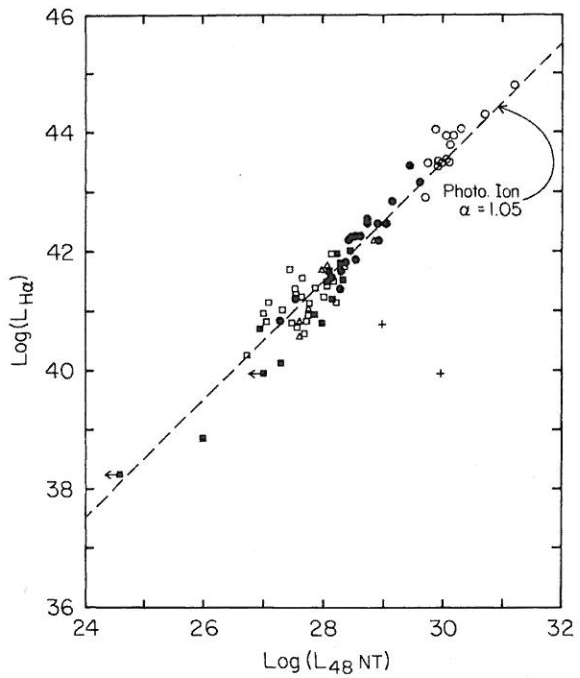

Fig. 28.21 The luminosity in the Hα emission line vs luminosity of the featureless continuum near 480 nm. NT stands for "nonthermal". The symbols are quasars (open circles), Seyfert 1s (filled circles), Seyfert 2s (open squares), NLRGs (triangles) & more Seyfert 2s & NLRGs (filled squares).

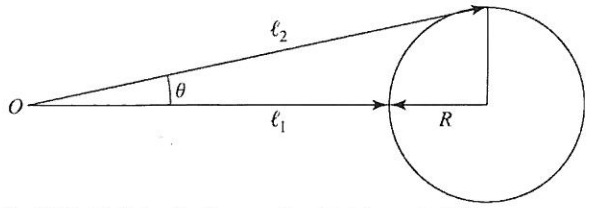

Fig. 28.22 The brightening of a sphere as seen by a distant observer at point O.

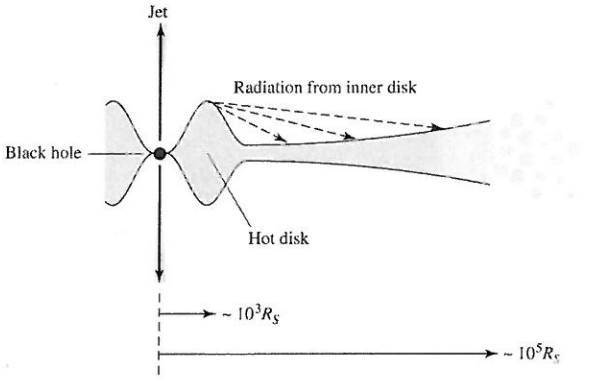

Fig. 28.23 A schematic structure of the accretion disk in an AGN. The radial direction is not drawn to scale.

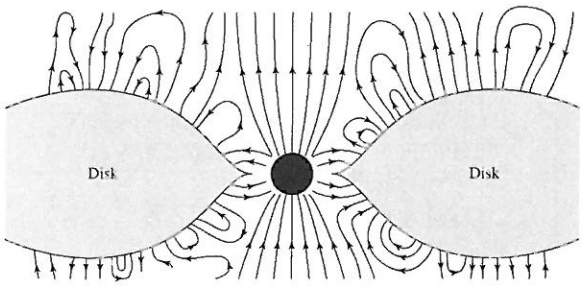

Fig. 28.24 An accretion disk & its magnetic field orbiting a rotating black hole.

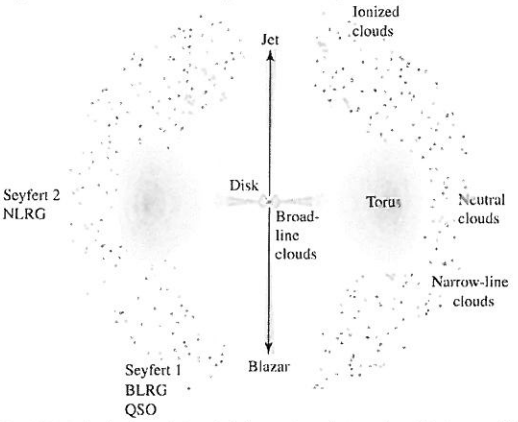

Fig. 28.25 A sketch of a unified model of an active galactic nucleus. The jets would be present in a radio-loud AGN. A typical observer's point of view is indicated for AGNs of various types.

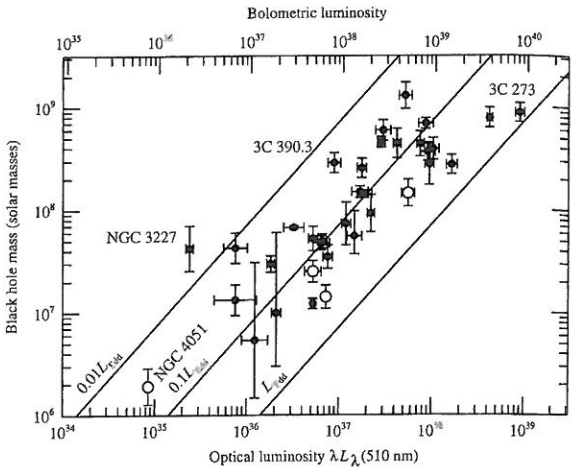

Fig. 28.26 The masses of the supermassive BHs in AGNs as a function of their luminosities. The solid diagonal lines represent lines of constant fractions of the Eddington luminosity.

This much mass in small $R \Rightarrow$ B.H.
$R_S = 7.2\,AU \Rightarrow M = \frac{Rc^2}{2G} = 3.7\times10^8\,M_\odot$
this is consistent, so for rest of 5.2.8.2 assume $M = 10^8 M_\odot$, $R_S = 2\,AU$.

p.1110 Generating Luminosity through Accretion
For NS, L generated when $\dot{M}$ hits hard surface.
BH doesn't have hard surface, $\dot{M}$ appears to slowly approach event horizon.
L generated in inner part of accretion disk.
$L_{disk} = \eta \dot{M} c^2$, $0.0572 \le \eta \le 0.423$
$\eta = 0.0572$ for nonrotating BH, 0.423 for maximally rotating BH.
Detailed calculations give Eq. 18.20 for characteristic temperature of disk:
$$T_{disk} = \left(\frac{3GMM}{8\pi\sigma R^3}\right)^{1/4}$$
Rapidly rotating BH $\Rightarrow R = 0.5 R_S = GM/c^2$.
For disk radiating at fraction $f_{Ed} = L_{disk}/L_{Ed}$ of L_{Ed},
$L = \eta \dot{M} c^2 = f_{Ed} L_{Ed} = f_{Ed} \frac{4\pi GMc}{\kappa} M \Rightarrow T_{disk} = \left(\frac{3c^5 f_{Ed}}{2\kappa\sigma GM\eta}\right)^{\frac{1}{4}}$
Note $T_{disk} \propto M^{-\frac{1}{4}}$

Ex. 28.2.1 p.1112 For $f_{Ed} = 1$, $\eta = 0.1$, $M = 10^8 M_\odot \Rightarrow L = 1.5\times10^{39}\,W$, $\dot{M} = 2.6\,M_\odot\,yr^{-1}$
$T_{disk} = 7.30\times10^5\,K \Rightarrow \lambda_{max} = 39.7\,nm$, extreme UV

Structure of the Accretion Disk p.1113
(Fig. 28.23) Explain all.

p.1114 the Implications of AGN Spectra – skip

Producing a Relativistic Outflow of Charged Particles
2 processes
(1) Similar to pulsars, but B produced by highly conducting rotating disk, then varying B produces E which accelerates particles to relativistic speeds.
(2) Blandford-Znajek mechanism – BH acts as spinning conductor in mag. field produces potential difference between poles & equator, effective resistance is 30 Ω, rotational energy of BH emitted as radiation & e^-e^+ pairs
$$P \simeq \frac{4\pi}{\mu_0} B^2 R_S^2 c = 2.7\times10^{38}\,W = 7.1\times10^{11}\,L_\odot \quad \text{for } B = 1\,T$$ (Fig. 28.24)
Some combination of these processes produces the relativistic outflow which can produce the observed synchrotron radiation.

p.1115 the Generation of X-rays
X-rays from AGNs are probably responsible for X-ray background.
X-rays are produced by the hot inner accretion disk.

p.1116 Broad-Line & Narrow-Line Emission
Emission lines formed by photoionization by continuum radiation.
It seems that broad & narrow lines are produced in different regions.

the Broad-Line Region

when continuum varies, broad line respond within ≤ 1 month $\Rightarrow R = ct = 10^{15}$ m $\Rightarrow$ relatively close to center,
Unified Model (Fig. 28.25) shows how different viewing angles could give various observed AGN types,
Example: Seyfert 2s have narrow lines only because broad line region is obscured by torus
Blazar produced when jet points towards observer,

p. 1117 ~~Determining BH Masses in Broad-Line Regions~~

Broad emission lines $\Rightarrow$ clouds orbit,
Width of line = 5000 km s^{-1} = orbital velocity, then $r = 10^{15}$ m $\Rightarrow M_{BH} = \frac{rv^2}{G} = 1.9 \times 10^8 M_\odot$
Time delay from continuum brightness changes to line changes $\Rightarrow$ reverberation mapping. $\Rightarrow$ (somehow) M_{BH} (Fig. 28.26) (lots of uncertainty)

p. 1118 The Narrow-Line Region

(Fig. 28.25) The narrow-line region seems to be a clumpy ~spherical distribution of gas w/ $T \sim 10^4$ K
Ex. 28.2.2 (skip) estimates the filling factor to be ~ 0.02 – clouds occupy 2% of volume,
(Fig. 28.27) Explain caption. Flow could be driven by radiation pressure, wind from accretion disk, or could be part of jet.

p. 1121 A Summary of the Unified Model of AGNs

Central engine is accretion disk orbiting rotating SMBH.
Powered by conversion of grav. P.E. into synchrotron rad., & maybe also rotational K.E. of BH.
$\dot{M} = 1\text{–}10\ M_\odot\ \text{yr}^{-1}$.
Observation angle, $\dot{M}$, & M_{SMBH} determine whether AGN is Seyfert 1 or 2, BLRG (broad-line radio galaxy), NLRG, or radio-loud vs. quiet quasar.
(Fig. 28.28) HST image of elliptical radio galaxy NGC 4261.
$M_{SMBH} \sim 10^7 M_\odot$, $r_{torus} \sim 70$ pc, jets extend to 15 kpc.
($R_s \sim 3 \times 10^{10}$ m < 1mm on photo).

Ch. 29 Cosmology

§29.1 Newtonian Cosmology p. 1144

Cosmology is the study of the origin & evolution of the universe.
In this section we will develop our intuition by using Newtonian physics, w/o GR or particle physics.

Olber's Paradox p. 1145

Newton believed in an infinite static universe filled uniformly w/ stars.

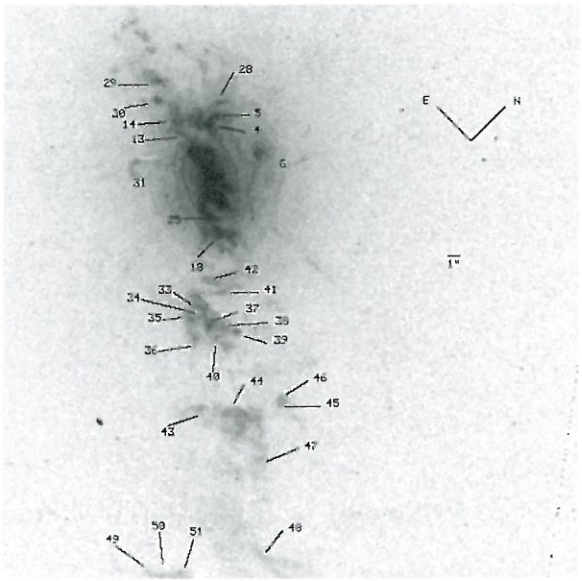

Fig. 28.27 An HST image of the narrow-line region of the Seyfert 1 galaxy NGC 4151. Numerous clouds are evident in a biconical distribution. The clouds in the SW are approaching the observer relative to the nucleus, & the clouds in the NE have recessional velocities. There is some evidence that the clouds may be associated with the galaxy's radio jets.

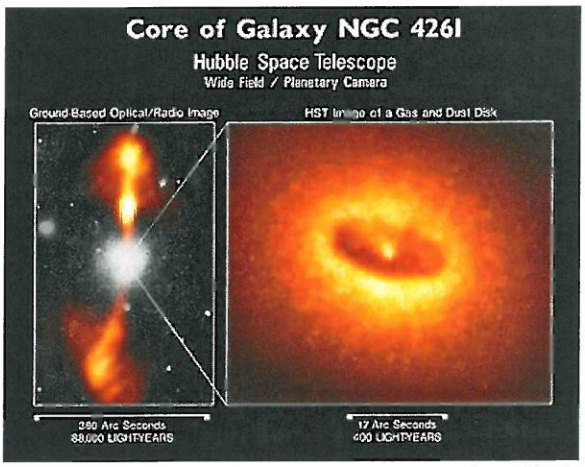

Fig. 28.28 Two views of NGC 4261. Left: a composite optical & radio image, showing the radio jets. Right: an optical image from HST, showing the dusty torus around the nucleus.

§28.3 starts here

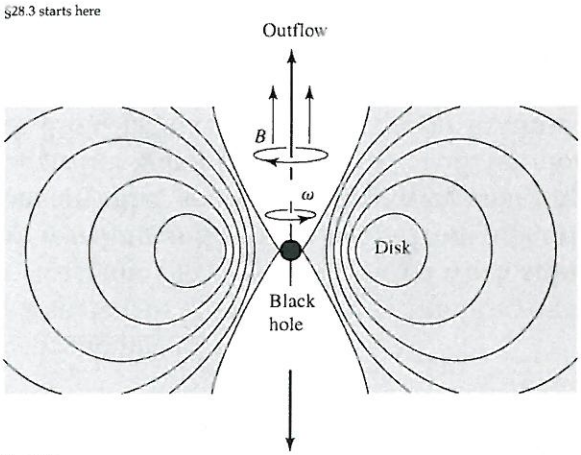

Fig. 28.29

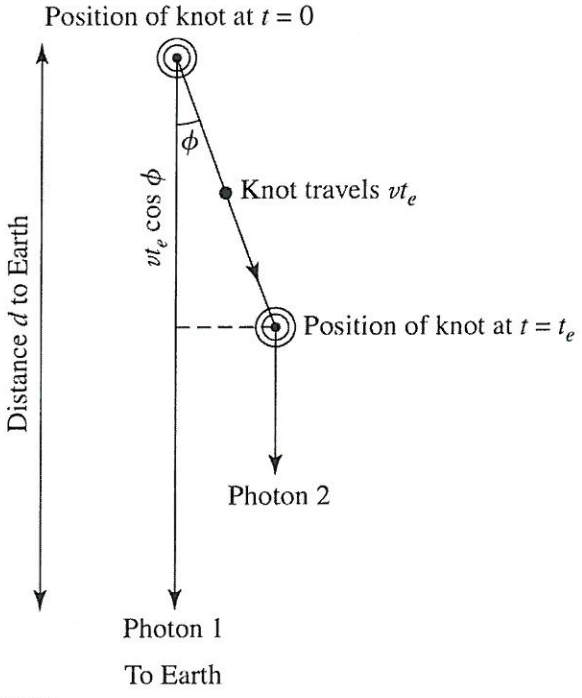

Fig. 28.32

60c 4/7/16

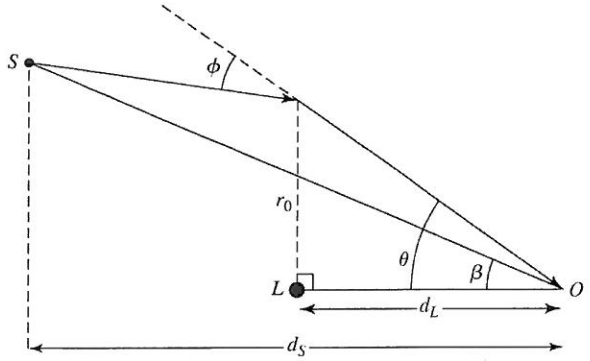

Fig. 28.35